Proceedings of Machine Learning Research vol 140:1–26, 2022 1st Conference on Causal Learning and Reasoning

Weakly Supervised Discovery of Semantic Attributes

Ameen Ali AMEENALI@MAIL.TAU.AC.IL
School of Computer Science
Tel Aviv University
Tel Aviv, Israel

Tomer Galanti GALANTI@MIT.EDU
Center for Brains, Minds and Machines (CBMM)
Massachusetts Institute of Technology
Cambridge, MA, USA

Evgenii Zheltonozhskii EVGENIIZH@CAMPUS.TECHNION.AC.IL
Department of Computer Science
Technion – Israel Institute of Technology
Haifa, Israel

Chaim Baskin CHAIMBASKIN@CS.TECHNION.AC.IL
Department of Computer Science
Technion – Israel Institute of Technology
Haifa, Israel

Lior Wolf WOLF@CS.TAU.AC.IL
School of Computer Science
Tel Aviv University
Tel Aviv, Israel

Editors: Bernhard Schölkopf, Caroline Uhler and Kun Zhang

Abstract

We consider the problem of extracting semantic attributes, using only classification labels for supervision. For example, when learning to classify images of birds into species, we would like to observe the emergence of features used by zoologists to classify birds. To tackle this problem, we propose training a neural network with discrete features in the last layer, followed by two heads: a multi-layered perceptron (MLP) and a decision tree. The decision tree utilizes simple binary decision stumps, thus encouraging features to have semantic meaning. We present a theoretical analysis, as well as a practical method for learning in the intersection of two hypothesis classes. Compared with various benchmarks, our results show an improved ability to extract a set of features highly correlated with a ground truth set of unseen attributes.

Keywords: Feature discovery, quantization, explainability

1. Introduction

The discovery of meaningful intermediate features in classification problems is at the heart of many scientific domains. For example, in botany, species are often identified based on dichotomous keys related to the shape of the leaf, the texture of the fruit, etc. (Project, 2021). In paleography, manuscripts are dated or attributed to a specific scribe based, among other attributes, on specific characteristics of the morphology of the letters (Stokes, 2009).

© 2022 A. Ali, T. Galanti, E. Zheltonozhskii, C. Baskin & L. Wolf.

Such intermediate features allow experts to discuss a certain classification outcome, for example, in case of an ambiguity or disagreement. Moreover, the attributes discovered help understand the underlying structure of the problem. In our paleography example, certain morphological attributes can be traced back to a specific school of scribes, and certain forms evolve over time in specific geographic locations, influenced by nearby writing cultures (James, 2020).

In this work, we define a weakly supervised attribute discovery problem, motivated by the nature of such intermediate level features. The problem is addressed within a novel theoretical framework, which gives rise to an effective method. Our focus is on binary attributes that are both evidence-based and distinctive. By evidence-based we mean that there is a mapping f such that every input x is mapped to a vector $f(x)$ of binary values, indicating the presence of each attribute. Distinctiveness means that there should be simple rules that determine the class label $y(x)$ based on the obtained attributes $f(x)$.

Currently, deep neural networks (DNNs) represent the most successful methodology for obtaining attributes from images (Zhang et al., 2014; Xu et al., 2020) and for classification. However, interpreting DNNs is very challenging (Zhang et al., 2021). In contrast, decision trees with binary decision stumps provide simple and interpretable decision rules, which are based on attributes (Guidotti et al., 2018). We propose merging the two approaches by training a DNN to produce quantized representations suitable for classification both by an MLP and by a decision tree.

To perform this hybrid learning task, we provide a theoretical analysis of the problem of learning at the intersection of two hypothesis classes. We study the optimization dynamics of training two hypotheses from two different classes of functions. The first one is trained to minimize its distance from the second one, and the second one is trained to minimize its distance from the first one and the target function. We call this process *Intersection Regularization*, since it regularizes the second hypothesis to be close to the first hypothesis class. We discuss the conditions on the loss surface in terms of theory, for which this process converges to an equilibrium point or a local minimum.

We present a method for concurrently training a network and a tree, based on the proposed analysis. The algorithm learns a quantized representation of the data and two classifiers on top of this representation: a decision tree and an MLP. The two classifiers are trained for a supervised multiclass classification task using intersection regularization. Our goal is to recover attributes that match those that humans would provide, without having access to such attributes during training. Since the human-defined attributes are typically sparse, we also apply L_1 regularization on the quantized vector of activations.

In an extensive set of experiments, we demonstrate that discrete representations, along with decision stumps learned using our algorithm, are highly correlated with a set of unseen human-defined attributes. At the same time, the overall classification accuracy is only slightly reduced compared to standard cross-entropy training.

The key contributions of this paper are as follows: (i) We identify a novel learning problem, which we call *Weakly Unsupervised Discovery of Semantic Attributes*. In this setting, samples are associated with abstract binary attributes and are labeled by class membership. The algorithm is provided with class-labeled samples and is assessed based on its ability to recover the binary attributes without any access to them. We provide concrete measures for testing the success of a given method for this task. (ii) We introduce a method for recovering the semantic attributes. This method is based on a novel regularization process for regularizing a neural network using a decision tree. We call this regularization method, *'Intersection Regularization'*, and (iii) We study the theory of convergence guarantees of the new regularization method to equilibrium points and local minima.

2. Related Work

Interpretability Developing tools and techniques to interpret existing deep learning based approaches and to build explainable machine learning algorithms is a fast-growing field of research. In computer vision, most contributions are concerned with providing an output relevance map. These methods include saliency-based methods (Simonyan et al., 2013; Zeiler and Fergus, 2014; Mahendran and Vedaldi, 2016; Zhou et al., 2016a; Dabkowski and Gal, 2017; Zhou et al., 2018; Gur et al., 2020), Activation Maximization (Erhan et al., 2009) and Excitation Backprop (Zhang et al., 2018), perturbation-based methods Fong and Vedaldi (2017); Fong et al. (2019). Shapley-value-based methods (Lundberg and Lee, 2017) enjoy theoretical justification and the Deep Taylor Decomposition (Montavon et al., 2017) provides a derivation that is also applicable to Layer-wise Relevance Propagation (LRP) (Bach et al., 2015) and its variants (Gu et al., 2018; Iwana et al., 2019; Nam et al., 2019) presented RAP. Gradient-based methods are based on the gradient with respect to the layer's input feature map and include Gradient*Input (Shrikumar et al., 2016), Integrated Gradients (Sundararajan et al., 2017), SmoothGrad (Smilkov et al., 2017), FullGrad (Srinivas and Fleuret, 2019), and Grad-CAM (Selvaraju et al., 2017).

Methods that provide an output relevance map suffer from several notable disadvantages. First, many of these methods were shown to suffer from a bias toward image edges and fail sanity checks that link their outcome to the classifiers, as shown by Asano et al. (2019). Furthermore, even though these methods are useful for visualization and downstream tasks, such as weakly supervised segmentation (Li et al., 2018), it is not obvious how to translate the image maps produced by these methods into semantic attributes, i.e., extract meaning from a visual depiction. An additional disadvantage of this approach is that it does not provide a direct method for evaluating whether a given neural network is interpretable or not, and the evaluation is often done with related tasks, such as segmentation or measuring the classifier's sensitivity to regions or pixels deemed important to the classification outcome or the absence of this. In our framework, we suggest objective measures in which one can quantify the degree of interpretability of a given model.

Since linear models are intuitively considered interpretable, Alvarez-Melis and Jaakkola (2018a) developed a framework in which the learned features are monotonic and additive. The explanation takes the form of presenting each attribute's contribution, explaining the attributes using prototype samples. Unlike our framework, no attempt was made to validate that the obtained attributes correspond to a predefined list of semantic attributes.

Local interpretability models, such as LIME (Ribeiro et al., 2016), approximate the decision surface for each specific decision by a linear model and, unlike our method, are not aimed at extracting meaningful attributes. Besides, such models are known to be sensitive to small perturbations of the input (Alvarez-Melis and Jaakkola, 2018b; Yeh et al., 2019).

Fine-Grained Classification Fine-grained classification aims at differentiating subordinate classes of a common superior class. Those subordinate classes are usually defined by domain experts, based on complicated rules, which typically focus on subtle differences in particular regions. Because of the inherent difficulty of classifying slightly different classes, many contributions in this area often aim at detecting informative regions in the input images that aid their classification (Duan et al., 2012; Yang et al., 2018; Chen et al., 2019; Hu et al., 2019; Huang and Li, 2020; Zhuang et al., 2020). In our work, we would like to recover semantic attributes that are not necessarily associated with specific image regions, e.g., mammal vs. reptile, or omnivore vs. carnivore.

Disentanglement A disentangled representation (Schmidhuber, 1992; Bengio et al., 2013a; Peters et al., 2017; Lake et al., 2017; Tschannen et al., 2018) is a representation that contains multiple independent parts. Various methods, such as (Brakel and Bengio, 2017; Feng et al., 2018; Marx et al., 2019; Tsai et al., 2020) have been able to effectively learn disentangled representations from data. This setting is different from ours in two ways. First, the attributes we would like to recover are not necessarily independent. Second, in disentanglement, we are typically interested in recovering any set of features that represent the data in a disentangled manner. In our case, success is measured subject to a specific set of attributes.

Attributes Discovery Attributes discovery has been an active research direction in computer vision. Attributes are typically referred as human-interpretable features that can describe the input image or the class it belongs to. Gutierrez et al. (2019) cast the problem of attributes discovery as a supervised learning task. Lampert et al. (2009); Farhadi et al. (2009a); Yu et al. (2013); Sattar et al. (2017) focus on category-level attributes, in which one would like to learn a set of attributes that describe the classes of the different images in the dataset. In several cases, and especially in fine-grained classification, predicting the class of an image is a more nuanced process, where the values of attributes may vary between images in the same category. In our paper, we focus on recovering instance-level attributes.

Explainability of Decision Trees Decision trees are known to be naturally explainable models, as long as the decision rules are easy to interpret. However, as far as we know, it has not been shown before that learning trees, while optimizing the features, lead to the emergence of attributes that are similar to those that appear in large set of (ground truth) relevant attributes.

In the context of the interpretability of recommendation systems, meta-trees were used for providing per-user decision rules (Shulman and Wolf, 2020). This method relies on a pre-existing set of features rather than extracting them from the input. In another line of work, Frosst and Hinton (2017) also employs preexisting features and distills the information within a deep network into a soft decision tree (Irsoy et al., 2012). Unlike our work, the neural network is not optimized to produce suitable features.

More relevant to our work is the Adaptive Neural Trees method of Tanno et al. (2019), which also combines decision trees and neural networks. In this method, trees of dynamic architectures that include network layers are grown so that the underlying network features gradually evolve. It is shown that the learned tree divides the classes along meaningful axes; however, the emergence of semantic attributes was not shown.

Quantization Quantization is the conversion of floating-point data to a low-bit discrete representation. The most common approaches for training a quantized neural network employ two sets of weights (Hubara et al., 2018; Zhou et al., 2016b). The forward pass is performed with quantized weights, and updates are performed on full precision ones, i.e., approximating gradients with the straight-through estimator (STE, Bengio et al., 2013b). In this work, we make use of quantizations in order to learn discrete, interpretable representations of the data within a neural network.

3. Problem Setup

In this section, we formulate a new learning setting, which we call *Weakly Unsupervised Discovery of Semantic Attributes*. In this setting, there is an unknown target function $y : \mathcal{X} \to \mathcal{Y}$, along with an attributes function $f : \mathcal{X} \to \mathcal{U}^d$ we would like to learn. Here, $\mathcal{X} \subset \mathbb{R}^n$ is a set of instances and $\mathcal{Y}$ is

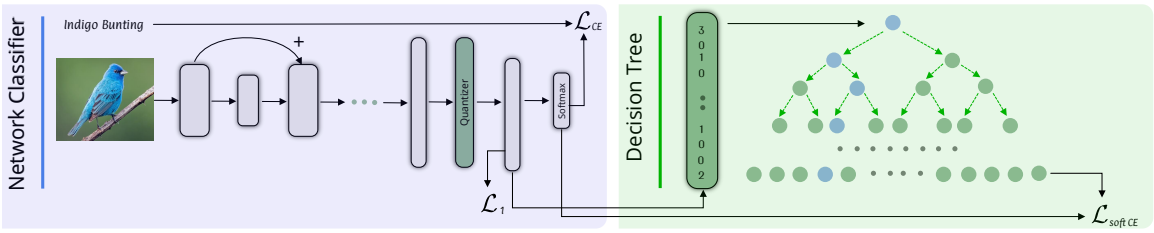

Figure 1: **An illustration of our method.** The model has three main components: **(a)** a quantized representation function F_q, **(b)** a classifier neural network G and **(c)** a multivariate decision tree T. We have three losses: a L_1 regularization loss over the masked quantized features, a cross-entropy loss between the network and the ground-truth labels, and a soft cross-entropy loss between the outputs of the tree and the network.

a set of labels. The function f is assumed to be d_0-sparse, i.e., $\forall x \in \mathcal{X}: \ \|f(x)\|_0 \leq d_0$. The values of f are taken from a latent space $\mathcal{U}^d$, where $\mathcal{U} = \mathbb{R}$, $[-1, 1]$ or $\{\pm 1\}$, depending on the task.

For example, $\mathcal{X}$ can be a set of images of k animal species and $\mathcal{Y} = \{\mathrm{e}_i\}_{i=1}^k$ the set of labels, where $\mathrm{e}_i \in \mathbb{R}^k$ is the i'th elementary vector. In this case, y is a classifier that takes an animal image x and returns the species of the animal. The function f corresponds to a set of d binary attributes $\{f_i\}_{i=1}^d$ (e.g., carnivore/herbivore). Each attribute f_i takes an image x and returns whether the animal illustrated in x satisfies the ith attribute.

Similarly to the standard learning setting, the set $\mathcal{X}$ is endowed with a distribution D, from which samples x are taken. The learning algorithm is provided with a set $\mathcal{S} = \{(x_i, y(x_i))\}_{i=1}^m$ of m i.i.d. samples. Typically, the learning algorithm is supposed to fit a hypothesis $H : \mathcal{X} \to \mathcal{Y}$ from a given *hypothesis class* $\mathcal{H}$ that would minimize the *expected risk*:

$$\mathcal{L}_D[H, y] := \mathbb{E}_{x \sim D}[\ell(H(x), y(x))], \tag{1}$$

where $\ell : \mathcal{Y}^2 \to [0, \infty)$ is a loss function, for example, the ℓ_2 loss function $\ell_2(a, b) = \|a - b\|_2^2$ for regression or the cross-entropy loss for classification. Since the algorithm is not provided with full access to D, it minimizes the empirical version of it

$$\mathcal{L}_{\mathcal{S}}[H, y] := \frac{1}{m} \sum_{(x, y(x)) \in \mathcal{S}} \ell(H(x), y(x)), \tag{2}$$

or minimizes $\mathcal{L}_{\mathcal{S}}[H, y]$ along with additional regularization terms.

In contrast to the standard learning setting, in our framework we would like to learn a model $H = G \circ q \circ F$ that minimizes the expected risk, but also recovers the semantic attributes $f(x)$ (without any access to these attributes). Here, F and G are a trainable representation function and a classifier, and q is a pre-defined discretization operator.

Put differently, the labels are given as proxy labels, while the actual goal is to learn a discrete-valued representation $q(F(x))$ of the data, which maximizes some measure of feature fidelity $d_D(F) = d_D(f; b \circ q \circ F)$ depending on the distribution D and a binarization function b that translates a vector into a binary vector (see Sec. 5 for details).

3.1. Measures of Feature Fidelity

The goal of training in the proposed setting is to learn a representation of the data $q(F(x))$ that maximizes the fidelity of the extracted features with respect to an unseen set of ground-truth binary attributes $f(x)$.

In this section, we define a generic family of functions $d_D(f; g)$ for measuring the fidelity of a multi-variate function $g : \mathcal{X} \to \mathcal{U}^d$ with respect to a multi-variate function $f : \mathcal{X} \to \mathcal{U}^n$ over a distribution D of samples.

Let $r(q_1, q_2; D)$ be a measure of accuracy between two univariate functions $q_1, q_2 : \mathcal{X} \to \mathcal{U}$ over a distribution D. In this paper, since we consider imbalanced attributes, r is the F1 score. Finally, we extend r to be annotation-invariant by using $\hat{r}(q_1, q_2; D) := \max\{r(q_1, q_2; D), r(q_1, 1 - q_2; D)\}$ as a measure of accuracy that is invariant to whether positive samples are denoted by 1 or 0.

Let $g : \mathcal{X} \to \{0, 1\}^d$ and $f : \mathcal{X} \to \{0, 1\}^n$ be two multivariate binary functions. We denote

$$d_D(f\|g) := \max_{\pi:[n]\to[d]} \frac{1}{n} \sum_{i=1}^{n} \hat{r}(f_i, g_{\pi(i)}; D) = \frac{1}{n} \sum_{i=1}^{n} \max_{j\in[d]} \hat{r}(f_i, g_j; D). \tag{3}$$

This quantity measures the average similarity between each feature f_i in f to some feature g_j in g.

The fidelity of g with respect to f is the harmonic mean $d_D(f; g) := 2\frac{d_D(f\|g)\cdot d_D(g\|f)}{d_D(f\|g)+d_D(g\|f)}$, which is a symmetric measure of similarity. Informally, $d_D(f\|g)$ measures the extent at which the set of attributes in f can be treated as a subset of the set of attributes in g and $d_D(f; g)$ as the extent at which the sets of attributes in f and g are equivalent. We use the harmonic mean as it penalizes low values, in contrast to the arithmetic mean.

When measuring the fidelity over a finite set of test samples $\mathcal{S}_T$, the proposed $d_D(f; g)$ considers the discrete uniform distribution $D = U[\mathcal{S}_T]$.

Finally, in some cases, it is more relevant to measure the distance between f and g instead of their similarity. We note that our method can be readily extended to this case by taking r to be a distance function and replacing the maximization in Eq. (3) and the definition of $\hat{r}$ by minimization. For example, for real-valued functions (i.e., $\mathcal{U} \subset \mathbb{R}$), it is reasonable to use the distance between the two functions, $r(q_1, q_2; D) = \mathbb{E}_{x\sim D}[|q_1(x) - q_2(x)|]$.

4. Intersection Regularization

A key component of our method in Sec. 5 is the proposed notion of *Intersection Regularization*. In this section, we introduce and study the optimization dynamics of the intersection regularization theoretically.

Suppose that we have two hypothesis classes $\mathcal{G} = \{G_\theta \mid \theta \in \Theta\}$ and $\mathcal{T} = \{T_\omega \mid \omega \in \Omega\}$, where Θ and Ω are two sets of parameters. Intersection regularization involves solving the following problem

$$\begin{aligned} &\min_{\theta\in\Theta} \min_{\omega\in\Omega} \mathcal{Q}(\theta, \omega) \\ &\text{where } \mathcal{Q}(\theta, \omega) := \mathcal{L}_{\mathcal{S}}[G_\theta, y] + \mathcal{L}_{\mathcal{S}}[G_\theta, T_\omega]. \end{aligned} \tag{4}$$

In this problem, we are interested in learning a hypothesis $G_\theta \in \mathcal{G}$ that is closest to the target function y among all members of $\mathcal{G}$ that can be approximated by a hypothesis $T_\omega \in \mathcal{T}$. We can think of $\mathcal{T}$ as prior knowledge we have on the target function y. Therefore, in some sense, the term $\mathcal{L}_{\mathcal{S}}[G_\theta, T_\omega]$ acts as a regularization term that restricts G_θ to be close to the class $\mathcal{T}$.

In Sec. 5, we use intersection regularization to train a neural network G over a quantized representation that mimics a decision tree T and minimizes the classification error. In this case, the class $\mathcal{T}$ consists of decision trees of a limited depth (ω is a vector that allocates an encoding of the tree, including its structure and decision rules) and $\mathcal{G}$ is a class of neural networks of a fixed architecture (θ is a vector of the weights and biases of a given network). The underlying quantized representation thus obtained is suitable for classification by both a decision tree and a neural network.

The following analysis focuses on two main properties: finding a local minima of $\mathcal{Q}$ and arriving at an equilibrium point of $\mathcal{Q}$. An equilibrium point of $\mathcal{Q}$ is a pair (θ, ω), such that, $\mathcal{Q}(\hat{\theta}, \hat{\omega}) = \min_\theta \mathcal{Q}(\theta, \hat{\omega}) = \min_\omega \mathcal{Q}(\hat{\theta}, \omega)$. The proofs are given in the appendix and are based on Thm. 2.1.14 by Nesterov (2014) and the analysis by Song et al. (2017).

The following proposition shows that under certain conditions it is possible to converge to an equilibrium of $\mathcal{Q}(\theta, \omega)$ when iteratively optimizing θ and ω. To show this, we assume that $\mathcal{Q}$ is a convex function with respect to θ for any fixed value of ω. This is true, for example, when G_θ is the linearization of a wide neural network (Lee et al., 2019), which also serve as universal approximators (Ji et al., 2020). It has also been proven that the optimization dynamics of wide neural networks match the dynamics of their linearized version (Lee et al., 2019). In addition, we assume that one is able to compute a global minimizer ω of $\mathcal{L}_\mathcal{S}[G_\theta, T_\omega]$ for any θ. This is typically impossible, however, it is reasonable to assume that one is able to approximately minimize $\mathcal{L}_\mathcal{S}[G_\theta, T_\omega]$ with respect to ω if it is being optimized by a descent optimizer. Throughout the analysis, we assume that $\cup_{\omega \in \Omega} \arg\min_\theta \mathcal{Q}(\theta, \omega)$ is well-defined and bounded and that $\lim_{\theta:\ \|\theta\| \to \infty} \mathcal{L}_\mathcal{S}[G_\theta, y] = \infty$.

Proposition 1 *Assume that $\mathcal{Q}(\theta, \omega)$ is convex and β-smooth w.r.t θ for any fixed value of ω. Let θ_1 be an initialization and $\omega_1 \in \arg\min_\omega \mathcal{Q}(\theta_1, \omega)$. We define θ_t to be the weights produced after t iterations of applying Gradient Descent on $\mathcal{Q}(\theta, \omega_{t-1})$ over θ with learning rate $\mu < \beta^{-1}$ and $\omega_t = \arg\min_\omega \mathcal{Q}(\theta_{t-1}, \omega)$. Then, we have*

$$\lim_{t \to \infty} \mathcal{Q}(\theta_t, \omega_t) = \lim_{t \to \infty} \min_\theta \mathcal{Q}(\theta, \omega_t) = \lim_{t \to \infty} \min_\omega \mathcal{Q}(\theta_t, \omega).$$

The following proposition shows that if we apply Block Coordinate Gradient Descent (BCGD) in order to optimize θ and ω minimize $\mathcal{Q}(\theta, \omega)$ (starting at (θ_1, ω_1)), then they converge to a local minimum that is also an equilibrium point. The BCGD iteratively updates: $\theta_{t+1} = \theta_t - \mu \nabla \mathcal{Q}(\theta_t, \omega_t)$ and $\omega_{t+1} = \omega_t - \mu \nabla \mathcal{Q}(\theta_{t+1}, \omega_t)$. Throughout the analysis we assume that the sets $\cup_{\omega \in \Omega} \arg\min_\theta \mathcal{Q}(\theta, \omega)$ and $\cup_{\theta \in \Theta} \arg\min_\omega \mathcal{Q}(\theta, \omega)$ are well-defined and bounded.

Proposition 2 *Assume that $\mathcal{Q}(\theta, \omega)$ is a twice continuously differentiable, element-wise convex (i.e., convex w.r.t θ for any fixed value of ω and vice versa), Lipschitz continuous and β-smooth function, whose saddle points are strict. Let θ_t, ω_t be the weights produced after t iterations of applying BCGD on $\mathcal{Q}(\theta, \omega)$ with learning rate $\mu < \beta^{-1}$. (θ_t, ω_t) then converges to a local minimum $(\hat{\theta}, \hat{\omega})$ of $\mathcal{Q}$ that is also an equilibrium point.*

5. Method

In this section, we propose our method for dealing with the problem introduced in Sec. 3.

Algorithm 1 Intersection Regularization-based Sparse Attributes Discovery

Require: $\mathcal{S} = \{(x_i, y(x_i))\}_{i=1}^m$ - dataset; $\lambda_1, \lambda_2, \lambda_3$ - non-negative coefficients; I - number of epochs; s - batch size; A - Tree training algorithm (and splitting criteria);

1: Initialize F, G and $T =$ None;
2: Partition $\mathcal{S}$ into batches $Batches(\mathcal{S})$ of size s;
3: **for** $i = 1, \ldots, I$ **do**
4: $\quad \bar{\lambda}_2 = \mathbb{1}[i > 1] \cdot \lambda_2$;
5: $\quad \mathcal{S}' = \emptyset$;
6: $\quad$ **for** $B \in Batches(\mathcal{S})$ **do**
7: $\quad\quad$ Update G using GD to minimize $\lambda_1 \mathcal{L}_B[G \circ F_q, y] + \bar{\lambda}_2 \mathcal{L}_B[G \circ F_q, T \circ F_q]$;
8: $\quad\quad$ Update F using GD to minimize $\lambda_1 \mathcal{L}_B[G \circ F_q, y] + \bar{\lambda}_2 \mathcal{L}_B[G \circ F_q, T \circ F_q] + \lambda_3 \mathcal{R}_B[F]$;
9: $\quad\quad$ Extend $\mathcal{S}' = \mathcal{S}' \cup \{(F_q(x), G(F_q(x))) \mid x \in B\}$;
10: $\quad$ **end for**
11: $\quad$ Initialize decision tree T;
12: $\quad$ Train T over $\mathcal{S}'$ using A;
13: **end for**
14: **return** F, G, T;

Model Informally, our algorithm aims to learn a sparse discrete representation $F_q(x) := q(F(x))$ of the data, that is suitable for classification by a decision tree T of small depth. Intuitively, this leads to a representation that supports classification by relatively simple decision rules. For this purpose, we consider a model of the following form: $H_{tree} = T \circ F_q$, where $F : \mathcal{X} \to \mathbb{R}^d$ is a trainable neural network and $T : \mathbb{R}^d \to \mathbb{R}^k$ is a decision tree from a class $\mathcal{T}$ of multivariate regression decision trees of maximal depth $d_{\max}$. The function G (and T) is translated into a classifier by taking $\arg\max_{i \in [k]} G(F_q(x))$ (and $\arg\max_{i \in [k]} T(F_q(x))$).

In order to learn a neural network G that minimizes the classification error and also approximates a decision tree, we apply intersection regularization between a class of neural networks $\mathcal{G}$ and the class of decision trees $\mathcal{T}$. Our objective function is decomposed into several loss functions. For each loss, we specify in brackets "$[\ \cdot\ ]$" the components responsible for minimizing the specified loss functions. For a full description of our method, see Alg. 1.

For each epoch (line 3), we iteratively update the network to minimize its objective function using GD and train the decision tree from scratch. To optimize the neural network, we use two loss functions (lines 7-8). The first one is the cross-entropy loss of H_{net} with respect to the ground-truth labels, and the second one is the soft cross-entropy loss of H_{net} with respect to the probabilities of H_{tree},

$$\mathcal{L}_B[G \circ F_q, y] \text{ and } \mathcal{L}_B[G \circ F_q, T \circ F_q], \tag{5}$$

where the loss function $\ell : \Delta_k \times \Delta_k \to [0, \infty)$ is the cross-entropy loss defined as follows: $\ell(u, v) := -\sum_{i=1}^k v_i \cdot \log(u_i)$, k is the number of classes and Δ_k is the standard simplex. The second loss is applied only from the second epoch onwards (line 4).

To learn sparse representations (Tibshirani, 1996; Koh et al., 2007), we also apply L_1 regularization over the quantized representation of the data

$$\mathcal{R}_B[F] := \frac{1}{m} \sum_{i=1}^{s} \|F_q(x_i)\|_1. \tag{6}$$

Tree Optimization During each epoch, we accumulate a dataset $\mathcal{S}'$ of pairs $(F_q(x), G(F_q(x)))$ for all of the samples x incurred until the current iteration (line 9 in Alg. 1). By the end of the epoch, we train a multivariate regression decision tree T from scratch over the dataset $\mathcal{S}'$ (see line 12 in Alg. 1). To train the decision tree, we used the CART algorithm of Loh (2011) with the information gain splitting criteria.

Quantization and Binarization The function $F : \mathcal{X} \to \mathbb{R}^n$ is a real-valued multivariate function. To obtain a discrete representation of the data, we discretize the outputs of F using the uniform quantizer (Sheppard, 1897; Vanhoucke et al., 2011) q, see appendix B for a step-by-step listing of the algorithm. This quantization employs a finite number of equally sized bins. Their size is calculated by dividing the input range into 2^r bins, where r specifies the number of bits for encoding each bin.

Since the round function is non-differentiable, the gradients of the uniform quantization are usually approximated (Bengio et al., 2013b; Ramapuram and Webb, 2019; Yang et al., 2019). In this paper, we utilize the straight-through estimator (Bengio et al., 2013b), which assumes that the Jacobian of rounding is simply identity, to estimate gradients of the discretization.

For applying the feature fidelity measure proposed in Sec. 3.1, we first cast the discrete vector $q(F(x))$ into a vector of binary features $b(q(F(x)))$ and compute $d_D(F) := d_D(f; b \circ q \circ F)$, where b is a binarization function. In this paper, we use the following binarization scheme. For a given vector $v = q(F(x))$ we compute $u = b(v) := (u^1 \| u^2)$ as follows: for all $i \in [n]$ and $j \in [2^r]$, we have: $u^1_{i,j} = \mathbb{1}[v_i = j]$ and $u^2_{i,j} = \mathbb{1}[v_i \neq j]$, where $\mathbb{1}$ is the indicator function. The dimension of u is $2^{r+1} \cdot n$.

6. Experiments

In this section, we evaluate our method on several datasets with attributes in comparison to various baselines.

Implementation Details The architecture of the feature extractor F is taken from (Du et al., 2020) with the published hyperparameters and is based on ResNet-50 . The classifier G is a two-layered, fully connected neural network. We initialize the ResNet with pre-trained weights trained on ILSVRC2012 (Russakovsky et al., 2015). Finetuning a pre-trained model, instead of training the model from scratch is the common practice in fine-grained classification, for example Du et al. (2020); Zhuang et al. (2020) employ an imagenet trained backbone model and finetune it over the fine-grained classification task. If one trains any of these models (including ours) on fine-grained classification tasks without pre-training the model, the results for the classification accuracy will be lower, and we can expect the fidelity score to be lower, as well. When training our method and the baselines we employed the following early stopping criterion: we train the model until the second epoch for which the accuracy rate drops over a validation set, and report the results for the last epoch before the drop. In order to conduct a fair comparison we matched the original scheduler of Li et al. (2018)

Throughout the experiments, we used the following default hyperparameters, except in our ablation studies, where we varied the hyperparameters in order to evaluate their effect. The coefficients for the loss functions are $\lambda_1 = 2$, $\lambda_2 = 1$, $\lambda_3 = 0.001$. Optimization was carried out using SGD. We used batch size of 64 across all of the expermints, and 0.0001 as the learning rate . For the data augmentations, RandomHorizontalFlip,RandomCrop are used with flipping probability $p = 0.5$.

Datasets Our experiments employed the following datasets: (i) The aYahoo dataset (Farhadi et al., 2009b), consisting of 1850 training and 794 test images from 12 classes (e.g., bag, goat, mug). Each image is labeled with 64 binary attributes. The images are collected from Yahoo. (ii) a Pascal dataset (Farhadi et al., 2009b) consisting of 20 classes and 2869 training and 2227 test images. The images are labeled with the same 64 binary attributes as in the aYahoo dataset. (iii) Animals with attributes dataset (AwA2) (Xian et al., 2018) consisting of 26125 training and 11197 test images from 50 animal classes, where each class is labeled with 85 numeric attribute values, (iv) CUB-200-2011 (Wah et al., 2011) consisting of 200 bird species classes, where each image out of 5993 training and 5794 test images is labeled with 312 binary attribute values. We used the standard train/evaluation splits of the datasets.

Runtime and Infrastructure The experiments were run on three GeForce RTX 3090 GPUs. Our method completes an epoch every 7 minutes on aYahoo, 10 minutes on aPascal, 1 hour on AwA2, and 1 hour on CUB-200-2011. On average, our method runs for approximately 12 epochs on both aYahoo and aPascal, 2-4 epochs on AwA2, and 35-40 on CUB-200-2011. The exact time withing this range depends on the representation capacity (e.g., number of bits, dimension).

Baseline methods We compare our method with various methods that capture a wide variety of approaches: (i) SDT (Frosst and Hinton, 2017) and ANT (Tanno et al., 2019), train a neural network of a tree architecture with the intention of learning high-level concepts. (ii) WS-DAN (Hu et al., 2019) is a method that generates attention maps representing the object's discriminative parts in order to improve the classification. (iii) DFL-CNN and Nts (Wang et al., 2018; Yang et al., 2018) use a network that captures class-specific discriminative regions. Region Grouping (Huang and Li, 2020) is a similar method, which also uses a regularization term that enforces the empirical distribution of part occurrence to align a U-shaped prior distribution. (iv) ProtoPNet (Chen et al., 2019) computes similarity scores of informative patches in the image with learned prototype images. These similarity scores are then aggregated by an MLP classifier. All baselines, except ProtoPNet, are provided with labeled samples, without access to ground-truth semantic segmentation of any kind. ProtoPNet employs cropping-based pre-processing that makes use of the bounding boxes provided with the CUB-200-2011 dataset.

To measure the baselines' and our method's performance on our task, we apply quantization to the penultimate layer of each model. For each method, we apply configurations with penultimate layer dimension $128, 256$ or 512 and apply uniform quantization with a $1, 2, 3$ or 4-bit representation. We report, for each method, the results of the configuration that provides the highest accuracy rate on the validation set. Note that this selection is based on accuracy, not on the feature fidelity score. The fidelity score is computed as follows: $d_D(F) := d_D(f; b \circ q \circ F)$, where F is the penultimate layer of the model and q, b are the uniform quantization and binarization operators.

Quantitative Analysis In Tab. 1 we report the results of our method and of the various baselines for each dataset. As can be seen, our method obtains a significantly higher feature fidelity score than the baselines across all datasets. We note that ProtoPNet (Chen et al., 2019) makes use of cropping-based preprocessing. In order to compare its results with those of the other methods fairly, we omitted pre-processing on all datasets, except for CUB-200-2011. As can be seen, our method achieves a fidelity score that is higher than ProtoPNet's on CUB-200-2011, even though this kind of supervision helps ProtoPNet achieve the most competitive feature fidelity score among the baselines.

Table 1: **Comparing the performance of various baselines with our method.** We report the classification accuracy rate (Acc) and the feature fidelity score ($d_D(F)$) for each method on each odataset. For ProtoPNet on CUB-200-2011, we report the results with (right) and without (left) using cropping-based augmentations. As can be seen, our method outperforms the other methods in terms of recovering the semantic attributes across datasets.

	CUB-200-2011				aYahoo				AwA2				aPascal			
Method	Bits	Dim	Acc	$d_D(F)$	Bits	Dim	Acc	$d_D(F)$	Bits	Dim	Acc	$d_D(F)$	Bits	Dim	Acc	$d_D(F)$
SDT	4	512	9.80%	33.01	3	512	17.58%	31.90	2	256	7.21%	66.17	2	128	30.48%	31.53
ANT	2	512	11.13%	33.69	4	512	35.66%	39.35	3	256	14.17%	69.27	3	256	31.70%	39.24
PMG	4	512	86.41%	39.06	3	512	96.14%	43.68	1	256	96.14%	71.70	2	128	**79.22%**	45.82
WS-DAN	4	256	87.54%	37.90	2	256	96.82%	56.90	4	512	96.22%	78.08	3	512	79.03%	57.44
DFL-CNN	3	512	85.88%	37.56	3	512	88.16%	30.06	4	256	89.20%	65.01	4	256	72.82%	43.13
Nts	2	128	85.42%	40.66	3	128	98.11%	55.27	4	256	96.12%	79.40	3	128	76.10%	53.42
API-Net	3	512	**88.21%**	36.77	3	512	**98.72%**	57.26	4	256	**96.25%**	79.85	3	256	79.15%	57.58
ProtoPNet	3	512	78.82%	35.31	4	256	85.62%	49.67	2	512	89.11%	76.42	2	512	73.52%	49.66
Region Group	3	512	86.10%	40.45	2	512	97.70%	58.90	3	512	96.11%	80.27	3	256	77.27%	56.80
Quantized network	4	512	80.08%	40.22	1	512	98.08%	55.75	2	512	95.30%	80.32	2	256	74.80%	56.30
Quantized net + DT	4	512	39.04%	32.11	1	512	58.24%	35.77	2	512	52.09%	68.77	2	256	47.65%	33.82
Quantized net + L1	4	512	80.61%	41.82	1	512	97.57%	59.20	2	512	94.81%	83.31	2	256	75.06%	59.80
Our method	4	512	79.82%	**42.58**	1	512	96.86%	**61.46**	2	512	94.48%	**84.67**	2	256	75.09%	**61.72**

On the other datasets, where no such crops were available, and where ProtoPNet is trained on the entire frame, the feature fidelity score of ProtoPNet is significantly worse than that of our method.

Ablation Study We conducted several ablation studies in order to validate the soundness of our method. Throughout the ablations, we compared our method with three of its variations: (i) a quantized network trained to minimize the cross-entropy loss, (ii) a quantized network trained to minimize the cross-entropy loss and the L_1 regularization loss and (iii) a quantized network with a differentiable soft decision tree (SDT) on top of it, trained to minimize the cross-entropy loss. In all three cases, the neural network is initialized with weights pre-trained on ILSVRC2012 (Russakovsky et al., 2015). We used the online learning decision trees of Domingos and Hulten (2000). The quantized network uses the same architecture as our model and is trained with the same hyperparameters.

As can be seen in Tab. 1, our method significantly improves the discovery of the semantic attributes, at the small expense of a slight decrease in classification accuracy, which is a secondary priority for our task.

To validate that the obtained performance gap in the fidelity score $d_D(F)$ is consistent across multiple configurations, we report in Fig 2 the results of the quantized neural network baseline method and our complete method. In Fig 3, we report the obtained classification accuracy per classification. As can be seen, our method does not harm the models' accuracy, while it generally improves the feature fidelity score across the various configurations of feature dimensions and the number of bits used in the binarization process.

A qualitative analysis of the attributes that emerge within the learned representations when our full method is applied is presented in Appendix C. A short study of the training dynamics of the Intersection Regularization loss, CE loss, accuracy and fidelity score is provided in Appendix D.

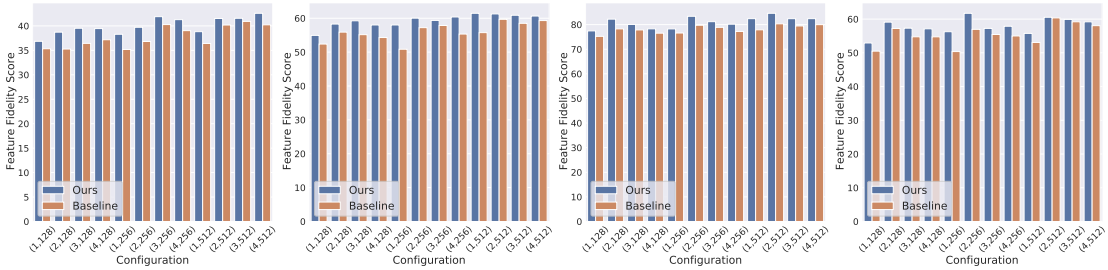

(a) CUB-200-201 (b) aYahoo (c) AwA2 (d) aPascal

Figure 2: Comparing the performance of our method (blue) and a standard quantized neural network (orange) with respect to the feature fidelity score ($d_D(F)$). The results are shown for different configurations of feature dimensions n and number of bits k for binarization, labeled as (n, k).

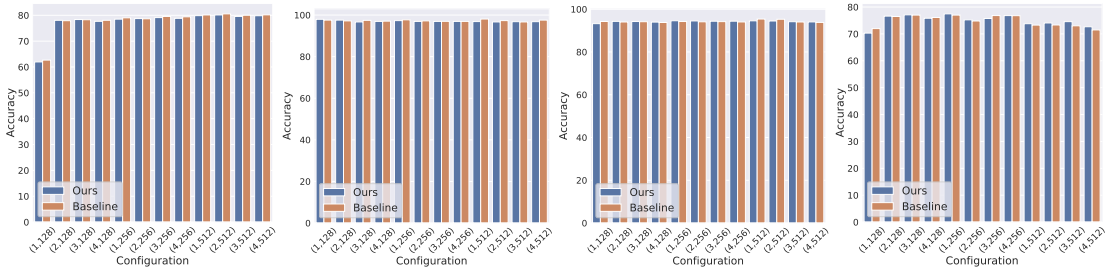

(a) CUB-200-201 (b) aYahoo (c) AwA2 (d) aPascal

Figure 3: Comparing the performance of our method (blue) and a standard quantized neural network (orange) with respect to classification accuracy rate. The results are shown for each configuration (n, k), where n is the feature dimension and k is the number of quantization bits.

7. Limitations

There are a few limitations to both our problem setting and algorithmic approach. First, the problem of "Weakly Supervised Discovery of Semantic Attributes" discussed in Sec. 3 is ill-posed in the general case. This is because we do not have access to the ground-truth binary attributes, and potentially the function $f(x)$ could be replaced with a different function, even when assuming that $y(x)$ is a function of $f(x)$. For example, in general, if $y(x) = \text{sign}(\sum_i f(x)_i)$, then, there are typically multiple functions $f(x)$ that could implement $y(x)$.

In particular, it is typically unknown what the dimension of F ought to be. This is no different from other unsupervised learning settings, such as clustering (Shalev-Shwartz and Ben-David, 2014; Ben-David, 2018), cross-domain mapping (He et al., 2016; Zhu et al., 2017; Kim et al., 2017; Galanti et al., 2018), domain adaptation (Ben-David et al., 2006; Mansour, 2009; Mansour et al., 2009; Ben-David et al., 2010), causality and disentanglement (Peters et al., 2017; Locatello et al., 2019) and sparse dictionary learning (Hillar and Sommer, 2015; Garfinkle and Hillar, 2019), where ambiguity is an inherent aspect of the learning problem.

This issue makes this problem challenging, especially when the number of ground-truth attributes is large, as in the case of CUB-200-2011, or when there are multiple redundant attributes in the dataset.

To cope with the multiple-admissible-solution issue in unsupervised learning, one typically make assumptions on the structure of the target function, which narrows the space of functions captured by the algorithm. In our case, we assume that $y(x)$ can be represented as $t(f(x))$, where t is a decision tree of small depth.

8. Conclusions

In this paper, we introduced the problem of weakly supervised discovery of semantic attributes. This problem explores the emergence of interpretable features quantitatively, based on a set of semantic features that is unseen during training. We present evidence that methods which are tailored to extract semantic attributes do not necessarily perform well in this metric and suggest a new approach to solving this problem.

Our method is based on joint learning in the soft intersection of two hypothesis classes: a neural network for obtaining its classification power, and a decision tree for learning features that lend themselves to classification by short logical expressions. We demonstrate that this way of learning is more effective than other methods for the new task and that learning with the new regularization scheme improves the fidelity of the obtained feature map.

References

David Alvarez-Melis and Tommi S. Jaakkola. Towards robust interpretability with self-explaining neural networks. In S. Bengio, H. Wallach, H. Larochelle, K. Grauman, N. Cesa-Bianchi, and R. Garnett, editors, *Advances in Neural Information Processing Systems*, volume 31, pages 7775–7784. Curran Associates, Inc., 2018a.

David Alvarez-Melis and Tommi S. Jaakkola. On the robustness of interpretability methods. *arXiv preprint arXiv:1806.08049*, 2018b.

Yuki Markus Asano, Christian Rupprecht, and Andrea Vedaldi. A critical analysis of self-supervision, or what we can learn from a single image. *arXiv preprint arXiv:1904.13132*, 2019.

Sebastian Bach, Alexander Binder, Grégoire Montavon, Frederick Klauschen, Klaus-Robert Müller, and Wojciech Samek. On pixel-wise explanations for non-linear classifier decisions by layer-wise relevance propagation. *PloS one*, 10(7):e0130140, 2015.

Shai Ben-David. Clustering - what both theoreticians and practitioners are doing wrong. *Proceedings of the AAAI Conference on Artificial Intelligence*, 32(1), Apr. 2018.

Shai Ben-David, John Blitzer, Koby Crammer, and Fernando Pereira. Analysis of representations for domain adaptation. In *NIPS*, pages 137–144, 2006.

Shai Ben-David, John Blitzer, Koby Crammer, Alex Kulesza, Fernando Pereira, and Jennifer Wortman Vaughan. A theory of learning from different domains. *Machine Learning*, 79(1-2):151–175, 2010.

Yoshua Bengio, Aaron Courville, and Pascal Vincent. Representation learning: A review and new perspectives. *IEEE Trans. Pattern Anal. Mach. Intell.*, 35(8):1798–1828, August 2013a. ISSN 0162-8828. doi: 10.1109/TPAMI.2013.50.

Yoshua Bengio, Nicholas Léonard, and Aaron C. Courville. Estimating or propagating gradients through stochastic neurons for conditional computation. *CoRR*, abs/1308.3432, 2013b.

Philemon Brakel and Yoshua Bengio. Learning independent features with adversarial nets for non-linear ica, 2017.

Chaofan Chen, Oscar Li, Daniel Tao, Alina Barnett, Cynthia Rudin, and Jonathan K Su. This looks like that: Deep learning for interpretable image recognition. In H. Wallach, H. Larochelle, A. Beygelzimer, F. d'Alché-Buc, E. Fox, and R. Garnett, editors, *Advances in Neural Information Processing Systems*, volume 32. Curran Associates, Inc., 2019.

Piotr Dabkowski and Yarin Gal. Real time image saliency for black box classifiers. In *Advances in Neural Information Processing Systems*, pages 6970–6979, 2017.

Pedro Domingos and Geoff Hulten. Mining high-speed data streams. In *Proceedings of the Sixth ACM SIGKDD International Conference on Knowledge Discovery and Data Mining*, KDD '00, page 71–80, New York, NY, USA, 2000. Association for Computing Machinery. ISBN 1581132336.

Ruoyi Du, Dongliang Chang, Ayan Kumar Bhunia, Jiyang Xie, Zhanyu Ma, Yi-Zhe Song, and Jun Guo. Fine-grained visual classification via progressive multi-granularity training of jigsaw patches. In *European Conference on Computer Vision*, pages 153–168. Springer, 2020.

Kun Duan, Devi Parikh, David J. Crandall, and Kristen Grauman. Discovering localized attributes for fine-grained recognition. In *2012 IEEE Conference on Computer Vision and Pattern Recognition, Providence, RI, USA, June 16-21, 2012*, pages 3474–3481. IEEE Computer Society, 2012. doi: 10.1109/CVPR.2012.6248089. URL https://doi.org/10.1109/CVPR.2012.6248089.

Dumitru Erhan, Yoshua Bengio, Aaron Courville, and Pascal Vincent. Visualizing higher-layer features of a deep network. *University of Montreal*, 1341(3):1, 2009.

Ali Farhadi, Ian Endres, Derek Hoiem, and David Forsyth. Describing objects by their attributes. In *2009 IEEE Conference on Computer Vision and Pattern Recognition*, pages 1778–1785, 2009a. doi: 10.1109/CVPR.2009.5206772.

Ali Farhadi, Ian Endres, Derek Hoiem, and David Forsyth. Describing objects by their attributes. In *2009 IEEE Conference on Computer Vision and Pattern Recognition*, pages 1778–1785. IEEE, 2009b.

Zunlei Feng, Xinchao Wang, Chenglong Ke, Anxiang Zeng, Dacheng Tao, and Mingli Song. Dual swap disentangling. In *Proceedings of the 32nd International Conference on Neural Information Processing Systems*, NIPS'18, page 5898–5908, Red Hook, NY, USA, 2018. Curran Associates Inc.

Ruth C. Fong and Andrea Vedaldi. Interpretable explanations of black boxes by meaningful perturbation. In *Proceedings of the IEEE International Conference on Computer Vision*, pages 3429–3437, 2017.

Ruth C. Fong, Mandela Patrick, and Andrea Vedaldi. Understanding deep networks via extremal perturbations and smooth masks. In *Proceedings of the IEEE International Conference on Computer Vision*, pages 2950–2958, 2019.

Nicholas Frosst and Geoffrey Hinton. Distilling a neural network into a soft decision tree. *arXiv preprint arXiv:1711.09784*, 2017.

Tomer Galanti, Lior Wolf, and Sagie Benaim. The role of minimal complexity functions in unsupervised learning of semantic mappings. In *International Conference on Learning Representations*, 2018.

Charles J. Garfinkle and Christopher J. Hillar. On the uniqueness and stability of dictionaries for sparse representation of noisy signals. *IEEE Transactions on Signal Processing*, 67(23): 5884–5892, 2019. doi: 10.1109/TSP.2019.2935914.

Jindong Gu, Yinchong Yang, and Volker Tresp. Understanding individual decisions of cnns via contrastive backpropagation. In *Asian Conference on Computer Vision*, pages 119–134. Springer, 2018.

Riccardo Guidotti, Anna Monreale, Salvatore Ruggieri, Franco Turini, Fosca Giannotti, and Dino Pedreschi. A survey of methods for explaining black box models. *ACM computing surveys (CSUR)*, 51(5):1–42, 2018.

Shir Gur, Ameen Ali, and Lior Wolf. Visualization of supervised and self-supervised neural networks via attribution guided factorization. *arXiv preprint arXiv:2012.02166*, 2020.

Patricia Gutierrez, Pierre-Antoine Sondag, Petar Butkovic, Mauro Lacy, Jordi Berges, Felipe Bertrand, and Arne Knudson. Deep learning for automated tagging of fashion images. In Laura Leal-Taixé and Stefan Roth, editors, *Computer Vision – ECCV 2018 Workshops*, pages 3–11, Cham, 2019. Springer International Publishing. ISBN 978-3-030-11015-4.

Di He, Yingce Xia, Tao Qin, Liwei Wang, Nenghai Yu, Tie-Yan Liu, and Wei-Ying Ma. Dual learning for machine translation. In *Advances in Neural Information Processing Systems*. Curran Associates, Inc., 2016.

Christopher J. Hillar and Friedrich T. Sommer. When can dictionary learning uniquely recover sparse data from subsamples? *IEEE Transactions on Information Theory*, 61(11):6290–6297, 2015. doi: 10.1109/TIT.2015.2460238.

Tao Hu, Honggang Qi, Qingming Huang, and Yan Lu. See better before looking closer: Weakly supervised data augmentation network for fine-grained visual classification, 2019.

Zixuan Huang and Yin Li. Interpretable and accurate fine-grained recognition via region grouping. In *CVPR*, pages 8662–8672, 2020.

Itay Hubara, Matthieu Courbariaux, Daniel Soudry, Ran El-Yaniv, and Yoshua Bengio. Quantized neural networks: Training neural networks with low precision weights and activations. *Journal of Machine Learning Research*, 18(187):1–30, 2018.

Ozan Irsoy, Olcay Taner Yildiz, and Ethem Alpaydin. Soft decision trees. In *International Conference on Pattern Recognition*, 2012.

Brian Kenji Iwana, Ryohei Kuroki, and Seiichi Uchida. Explaining convolutional neural networks using softmax gradient layer-wise relevance propagation. *arXiv preprint arXiv:1908.04351*, 2019.

Kathryn James. *English Paleography and Manuscript Culture, 1500-1800*. Yale University Press, 2020.

Ziwei Ji, Matus Telgarsky, and Ruicheng Xian. Neural tangent kernels, transportation mappings, and universal approximation. In *International Conference on Learning Representations*, 2020. URL https://openreview.net/forum?id=HklQYxBKwS.

Taeksoo Kim, Moonsu Cha, Hyunsoo Kim, Jung Kwon Lee, and Jiwon Kim. Learning to discover cross-domain relations with generative adversarial networks. In *International Conference on Machine Learning (ICML)*, Proceedings of Machine Learning Research. PMLR, 2017.

Kwangmoo Koh, Seung-Jean Kim, and Stephen Boyd. An interior-point method for large-scale ℓ_1-regularized logistic regression. *Journal of Machine Learning Research*, 8(54):1519–1555, 2007.

Brenden M. Lake, Tomer D. Ullman, Joshua B. Tenenbaum, and Samuel J. Gershman. Building machines that learn and think like people. *Behavioral and Brain Sciences*, 40:e253, 2017. doi: 10.1017/S0140525X16001837.

Christoph H. Lampert, Hannes Nickisch, and Stefan Harmeling. Learning to detect unseen object classes by between-class attribute transfer. In *2009 IEEE Conference on Computer Vision and Pattern Recognition*, pages 951–958, 2009. doi: 10.1109/CVPR.2009.5206594.

Jaehoon Lee, Lechao Xiao, Samuel Schoenholz, Yasaman Bahri, Roman Novak, Jascha Sohl-Dickstein, and Jeffrey Pennington. Wide neural networks of any depth evolve as linear models under gradient descent. In H. Wallach, H. Larochelle, A. Beygelzimer, F. d'Alché-Buc, E. Fox, and R. Garnett, editors, *Advances in Neural Information Processing Systems*, volume 32. Curran Associates, Inc., 2019. URL https://proceedings.neurips.cc/paper/2019/file/0d1a9651497a38d8b1c3871c84528bd4-Paper.pdf.

Kunpeng Li, Ziyan Wu, Kuan-Chuan Peng, Jan Ernst, and Yun Fu. Tell me where to look: Guided attention inference network. In *Proceedings of the IEEE Conference on Computer Vision and Pattern Recognition*, pages 9215–9223, 2018.

Francesco Locatello, Stefan Bauer, Mario Lucic, Gunnar Raetsch, Sylvain Gelly, Bernhard Schölkopf, and Olivier Bachem. Challenging common assumptions in the unsupervised learning of disentangled representations. In Kamalika Chaudhuri and Ruslan Salakhutdinov, editors, *Proceedings of the 36th International Conference on Machine Learning*, volume 97 of *Proceedings of Machine Learning Research*, pages 4114–4124. PMLR, 09–15 Jun 2019.

Wei-Yin Loh. Classification and regression trees. *Wiley interdisciplinary reviews: data mining and knowledge discovery*, 1(1):14–23, 2011.

Scott M. Lundberg and Su-In Lee. A unified approach to interpreting model predictions. In *Advances in Neural Information Processing Systems*, pages 4765–4774, 2017.

Aravindh Mahendran and Andrea Vedaldi. Visualizing deep convolutional neural networks using natural pre-images. *International Journal of Computer Vision*, 120(3):233–255, 2016.

Yishay Mansour. Learning and domain adaptation. In *Algorithmic Learning Theory, 20th International Conference, ALT*, pages 4–6, 2009.

Yishay Mansour, Mehryar Mohri, and Afshin Rostamizadeh. Domain adaptation: Learning bounds and algorithms. In *COLT - The 22nd Conference on Learning Theory*, 2009.

Charles Marx, Richard Phillips, Sorelle Friedler, Carlos Scheidegger, and Suresh Venkatasubramanian. Disentangling influence: Using disentangled representations to audit model predictions. In H. Wallach, H. Larochelle, A. Beygelzimer, F. d'Alché-Buc, E. Fox, and R. Garnett, editors, *Advances in Neural Information Processing Systems*, volume 32. Curran Associates, Inc., 2019. URL https://proceedings.neurips.cc/paper/2019/file/55a988dfb00a914717b3000a3374694c-Paper.pdf.

Grégoire Montavon, Sebastian Lapuschkin, Alexander Binder, Wojciech Samek, and Klaus-Robert Müller. Explaining nonlinear classification decisions with deep taylor decomposition. *Pattern Recognition*, 65:211–222, 2017.

Woo-Jeoung Nam, Shir Gur, Jaesik Choi, Lior Wolf, and Seong-Whan Lee. Relative attributing propagation: Interpreting the comparative contributions of individual units in deep neural networks. *arXiv preprint arXiv:1904.00605*, 2019.

Yurii Nesterov. *Introductory Lectures on Convex Optimization: A Basic Course*. Springer Publishing Company, Incorporated, 1 edition, 2014. ISBN 1461346916.

J. Peters, D. Janzing, and B. Schölkopf. *Elements of Causal Inference: Foundations and Learning Algorithms*. MIT Press, Cambridge, MA, USA, 2017.

Jepson Flora Project. Jepson eFlora, 2021. URL https://ucjeps.berkeley.edu/eflora/.

Jason Ramapuram and Russ Webb. Improving discrete latent representations with differentiable approximation bridges, 2019.

Marco Tulio Ribeiro, Sameer Singh, and Carlos Guestrin. "Why should I trust you?": Explaining the predictions of any classifier. In *Proceedings of the 22Nd ACM SIGKDD International Conference on Knowledge Discovery and Data Mining*, KDD '16, pages 1135–1144, New York, NY, USA, 2016. ACM. ISBN 978-1-4503-4232-2.

Olga Russakovsky, Jia Deng, Hao Su, Jonathan Krause, Sanjeev Satheesh, Sean Ma, Zhiheng Huang, Andrej Karpathy, Aditya Khosla, Michael Bernstein, Alexander C. Berg, and Li Fei-Fei. Imagenet large scale visual recognition challenge. *Int. J. Comput. Vision*, 115(3):211–252, December 2015.

Hosnieh Sattar, Andreas Bulling, and Mario Fritz. Predicting the category and attributes of visual search targets using deep gaze pooling. In *Proceedings of the IEEE International Conference on Computer Vision (ICCV) Workshops*, Oct 2017.

Jürgen Schmidhuber. Learning factorial codes by predictability minimization. *Neural Comput.*, 4 (6):863–879, November 1992. ISSN 0899-7667. doi: 10.1162/neco.1992.4.6.863. URL https://doi.org/10.1162/neco.1992.4.6.863.

Ramprasaath R Selvaraju, Michael Cogswell, Abhishek Das, Ramakrishna Vedantam, Devi Parikh, and Dhruv Batra. Grad-cam: Visual explanations from deep networks via gradient-based localization. In *Proceedings of the IEEE international conference on computer vision*, pages 618–626, 2017.

Shai Shalev-Shwartz and Shai Ben-David. *Understanding Machine Learning: From Theory to Algorithms*. Cambridge University Press, New York, NY, USA, 2014. ISBN 1107057132, 9781107057135.

William Fleetwood Sheppard. On the calculation of the most probable values of frequency-constants, for data arranged according to equidistant division of a scale. *Proceedings of the London Mathematical Society*, 1(1):353–380, 1897.

Avanti Shrikumar, Peyton Greenside, Anna Shcherbina, and Anshul Kundaje. Not just a black box: Learning important features through propagating activation differences. *arXiv preprint arXiv:1605.01713*, 2016.

Eyal Shulman and Lior Wolf. Meta decision trees for explainable recommendation systems. In *Proceedings of the AAAI/ACM Conference on AI, Ethics, and Society*, AIES '20, page 365–371, New York, NY, USA, 2020. Association for Computing Machinery. ISBN 9781450371100.

Karen Simonyan, Andrea Vedaldi, and Andrew Zisserman. Deep inside convolutional networks: Visualising image classification models and saliency maps. *arXiv preprint arXiv:1312.6034*, 2013.

Daniel Smilkov, Nikhil Thorat, Been Kim, Fernanda Viégas, and Martin Wattenberg. Smoothgrad: removing noise by adding noise. *arXiv preprint arXiv:1706.03825*, 2017.

Enbin Song, Zhubin Shen, and Qingjiang Shi. Block coordinate descent only converge to minimizers, 2017.

Suraj Srinivas and François Fleuret. Full-gradient representation for neural network visualization. In *Advances in Neural Information Processing Systems*, pages 4126–4135, 2019.

Peter Stokes. Computer-aided palaeography, present and future. In Malte Rehbein, Torsten Schaßan, and Patrick Sahle, editors, *Kodikologie und Paläographie im digitalen Zeitalter - Codicology and Palaeography in the Digital Age*, volume 2, pages 309–338. BoD, Norderstedt, 2009.

Mukund Sundararajan, Ankur Taly, and Qiqi Yan. Axiomatic attribution for deep networks. In *Proceedings of the 34th International Conference on Machine Learning-Volume 70*, pages 3319–3328. JMLR. org, 2017.

Ryutaro Tanno, Kai Arulkumaran, Daniel Alexander, Antonio Criminisi, and Aditya Nori. Adaptive neural trees. In Kamalika Chaudhuri and Ruslan Salakhutdinov, editors, *Proceedings of the 36th International Conference on Machine Learning*, volume 97 of *Proceedings of Machine Learning Research*, pages 6166–6175. PMLR, 09–15 Jun 2019.

Robert Tibshirani. Regression shrinkage and selection via the lasso. *Journal of the Royal Statistical Society. Series B (Methodological)*, 58(1):267–288, 1996.

Yao-Hung Hubert Tsai, Han Zhao, Makoto Yamada, Louis-Philippe Morency, and Russ R Salakhutdinov. Neural methods for point-wise dependency estimation. In H. Larochelle, M. Ranzato, R. Hadsell, M. F. Balcan, and H. Lin, editors, *Advances in Neural Information Processing Systems*, volume 33, pages 62–72. Curran Associates, Inc., 2020. URL https://proceedings.neurips.cc/paper/2020/file/00a03ec6533ca7f5c644d198d815329c-Paper.pdf.

Michael Tschannen, Olivier Frederic Bachem, and Mario Lučić. Recent advances in autoencoder-based representation learning. In *Bayesian Deep Learning Workshop, NeurIPS*, 2018.

Vincent Vanhoucke, Andrew Senior, and Mark Z. Mao. Improving the speed of neural networks on cpus. In *Deep Learning and Unsupervised Feature Learning Workshop, NIPS 2011*, 2011.

Catherine Wah, Steve Branson, Peter Welinder, Pietro Perona, and Serge Belongie. The Caltech-UCSD Birds-200-2011 Dataset. Technical Report CNS-TR-2011-001, Caltech, 2011.

Yaming Wang, Vlad I. Morariu, and Larry S. Davis. Learning a discriminative filter bank within a CNN for fine-grained recognition. In *Proceedings of the IEEE Conference on Computer Vision and Pattern Recognition (CVPR)*, June 2018.

Yongqin Xian, Christoph H. Lampert, Bernt Schiele, and Zeynep Akata. Zero-shot learning—a comprehensive evaluation of the good, the bad and the ugly. *IEEE Transactions on Pattern Analysis and Machine Intelligence*, 41(9):2251–2265, 2018.

Wenjia Xu, Jiuniu Wang, Yang Wang, Yirong Wu, and Zeynep Akata. Generating visual and semantic explanations with multi-task network. In *European Conference on Computer Vision*, pages 620–635. Springer, 2020.

Jiwei Yang, Xu Shen, Jun Xing, Xinmei Tian, Houqiang Li, Bing Deng, Jianqiang Huang, and Xiansheng Hua. Quantization networks. In *Proceedings of the IEEE/CVF Conference on Computer Vision and Pattern Recognition (CVPR)*, June 2019.

Ze Yang, Tiange Luo, Dong Wang, Zhiqiang Hu, Jun Gao, and Liwei Wang. Learning to navigate for fine-grained classification. In *Proceedings of the European Conference on Computer Vision (ECCV)*, September 2018.

Chih-Kuan Yeh, Cheng-Yu Hsieh, Arun Sai Suggala, David Inouye, and Pradeep Ravikumar. How sensitive are sensitivity-based explanations? *arXiv preprint arXiv:1901.09392*, 2019.

Felix X. Yu, Liangliang Cao, Rogerio S. Feris, John R. Smith, and Shih-Fu Chang. Designing category-level attributes for discriminative visual recognition. In *Proceedings of the IEEE Conference on Computer Vision and Pattern Recognition (CVPR)*, June 2013.

Matthew D Zeiler and Rob Fergus. Visualizing and understanding convolutional networks. In *European conference on computer vision*, pages 818–833. Springer, Cham, 2014.

Jianming Zhang, Sarah Adel Bargal, Zhe Lin, Jonathan Brandt, Xiaohui Shen, and Stan Sclaroff. Top-down neural attention by excitation backprop. *International Journal of Computer Vision*, 126 (10):1084–1102, 2018.

Ning Zhang, Manohar Paluri, Marc'Aurelio Ranzato, Trevor Darrell, and Lubomir Bourdev. Panda: Pose aligned networks for deep attribute modeling. In *Proceedings of the IEEE conference on computer vision and pattern recognition*, pages 1637–1644, 2014.

Yu Zhang, Peter Tiňo, Aleš Leonardis, and Ke Tang. A survey on neural network interpretability. *IEEE Transactions on Emerging Topics in Computational Intelligence*, 2021.

Bolei Zhou, Aditya Khosla, Agata Lapedriza, Aude Oliva, and Antonio Torralba. Learning deep features for discriminative localization. In *Proceedings of the IEEE conference on computer vision and pattern recognition*, pages 2921–2929, 2016a.

Bolei Zhou, David Bau, Aude Oliva, and Antonio Torralba. Interpreting deep visual representations via network dissection. *IEEE transactions on pattern analysis and machine intelligence*, 2018.

Shuchang Zhou, Yuxin Wu, Zekun Ni, Xinyu Zhou, He Wen, and Yuheng Zou. Dorefa-net: Training low bitwidth convolutional neural networks with low bitwidth gradients. *arXiv preprint arXiv:1606.06160*, 2016b.

Jun-Yan Zhu, Taesung Park, Phillip Isola, and Alexei A. Efros. Unpaired image-to-image translation using cycle-consistent adversarial networks. In *International Conference on Computer Vision (ICCV)*. IEEE Computer Society, 2017.

Peiqin Zhuang, Yali Wang, and Yu Qiao. Learning attentive pairwise interaction for fine-grained classification. In *AAAI*, pages 13130–13137, 2020.

Appendix A. Proofs of Props. 1 and 2

Proposition 1 *Assume that $\mathcal{Q}(\theta, \omega)$ is convex and β-smooth w.r.t θ for any fixed value of ω. Let θ_1 be an initialization and $\omega_1 \in \arg\min_\omega \mathcal{Q}(\theta_1, \omega)$. We define θ_t to be the weights produced after t iterations of applying Gradient Descent on $\mathcal{Q}(\theta, \omega_{t-1})$ over θ with learning rate $\mu < \beta^{-1}$ and $\omega_t = \arg\min_\omega \mathcal{Q}(\theta_{t-1}, \omega)$. Then, we have*

$$\lim_{t\to\infty} \mathcal{Q}(\theta_t, \omega_t) = \lim_{t\to\infty} \min_\theta \mathcal{Q}(\theta, \omega_t) = \lim_{t\to\infty} \min_\omega \mathcal{Q}(\theta_t, \omega).$$

Proof First, we would like to prove that $\mathcal{Q}(\theta_t, \omega_t)$ is monotonically decreasing. We notice that for each $t \in \mathbb{N}$, we have

$$\mathcal{Q}(\theta_t, \omega_t) \leq \mathcal{Q}(\theta_t, \omega_{t-1}) \tag{7}$$

since ω_t is the global minimizer of $\mathcal{Q}(\theta_t, \omega)$. In addition, by the proof of (cf. Nesterov (2014), Thm. 2.1.14), we have

$$\mathcal{Q}(\theta_t, \omega_{t-1}) \leq \mathcal{Q}(\theta_{t-1}, \omega_{t-1}) - \eta \|\nabla_\theta \mathcal{Q}(\theta_t, \omega_{t-1})\|_2^2 \leq \mathcal{Q}(\theta_{t-1}, \omega_{t-1}), \tag{8}$$

where $\eta := \mu(1 - 0.5\beta\mu) > 0$. Therefore, we conclude that $\mathcal{Q}(\theta_t, \omega_t)$ is indeed monotonically decreasing. Since $\mathcal{Q}$ is non-negative, we conclude that $\mathcal{Q}(\theta_t, \omega_t)$ is a convergent sequence. In

particular, θ_t is bounded. Otherwise, $\mathcal{Q}(\theta_t, \omega_t) \geq \mathcal{L}_{\mathcal{S}}[h_{\theta_t}, y] \to \infty$ in contradiction to the fact that $\mathcal{Q}(\theta_t, \omega_t)$ is a convergent sequence.

Next, by applying the convexity of $\mathcal{Q}(\theta, \omega_{t-1})$ (as a function of θ), we have

$$\mathcal{Q}(\theta_t, \omega_{t-1}) - \mathcal{Q}(\theta_t^*, \omega_{t-1}) \leq \langle \nabla_\theta \mathcal{Q}(\theta, \omega_{t-1}), \theta_t - \theta_t^* \rangle \leq \|\nabla_\theta \mathcal{Q}(\theta_t, \omega_{t-1})\|_2 \cdot \|\theta_t - \theta_t^*\|_2, \quad (9)$$

where $\theta_t^* = \arg\min_\theta \mathcal{Q}(\theta, \omega_t)$. By combining Eqs. (8) and (9), we have

$$\mathcal{Q}(\theta_t, \omega_t) \leq \mathcal{Q}(\theta_t, \omega_{t-1}) \leq \mathcal{Q}(\theta_{t-1}, \omega_{t-1}) - \frac{\eta}{\|\theta_t - \theta_t^*\|_2^2} \left(\mathcal{Q}(\theta_{t-1}, \omega_{t-1}) - \min_\theta \mathcal{Q}(\theta, \omega_{t-1}) \right)^2 \quad (10)$$

In particular,

$$\mathcal{Q}(\theta_{t-1}, \omega_{t-1}) - \mathcal{Q}(\theta_t, \omega_t) \geq \frac{\eta}{\|\theta_t - \theta_t^*\|_2^2} \left(\mathcal{Q}(\theta_{t-1}, \omega_{t-1}) - \min_\theta \mathcal{Q}(\theta, \omega_{t-1}) \right)^2 \quad (11)$$

Since the left-hand side tends to zero and the right-hand side is lower bounded by zero, by the sandwich theorem the right-hand side tends to zero as well. Since both θ_t and θ_t^* are bounded sequences ($\{\arg\min_\theta \mathcal{Q}(\theta, \omega) \mid \omega \in \Omega\}$ is well-defined and bounded), we conclude that $\lim_{t\to\infty} \mathcal{Q}(\theta_t, \omega_t) = \lim_{t\to\infty} \min_\theta \mathcal{Q}(\theta, \omega_t)$. We also have: $\mathcal{Q}(\theta_t, \omega_t) = \min_\omega \mathcal{Q}(\theta_t, \omega)$ by definition, and therefore, $\lim_{t\to\infty} \mathcal{Q}(\theta_t, \omega_t) = \lim_{t\to\infty} \min_\omega \mathcal{Q}(\theta_t, \omega)$ as well. ■

Proposition 2 *Assume that $\mathcal{Q}(\theta, \omega)$ is a twice continuously differentiable, element-wise convex (i.e., convex w.r.t θ for any fixed value of ω and vice versa), Lipschitz continuous and β-smooth function, whose saddle points are strict. Let θ_t, ω_t be the weights produced after t iterations of applying BCGD on $\mathcal{Q}(\theta, \omega)$ with learning rate $\mu < \beta^{-1}$. (θ_t, ω_t) then converges to a local minimum $(\hat{\theta}, \hat{\omega})$ of $\mathcal{Q}$ that is also an equilibrium point.*

Proof Firstly, since $\mathcal{Q}(\theta, \omega)$ is a twice continuously differentiable, Lipschitz continuous and β-smooth function, by Prop. 3.4 and Cor. 3.1 in (Song et al., 2017), (θ_t, ω_t) converge to a local minimum $(\hat{\theta}, \hat{\omega})$ of $\mathcal{Q}$. Therefore, it is left to show that $(\hat{\theta}, \hat{\omega})$ is also an equilibrium point. We note that $\mathcal{Q}(\theta, \omega)$ is element-wise convex and β-smooth. By the proof of (cf. Nesterov (2014), Thm. 2.1.14), we have

$$\mathcal{Q}(\theta_{t+1}, \omega_t) \leq \mathcal{Q}(\theta_t, \omega_t) - \eta \|\nabla_\theta \mathcal{Q}(\theta_t, \omega_t)\|_2^2, \quad (12)$$

where $\eta := \mu(1 - 0.5\beta\mu) > 0$. By applying the convexity of $\mathcal{Q}(\theta, \omega_t)$ (as a function of θ), we have

$$\begin{aligned} \mathcal{Q}(\theta_t, \omega_t) - \mathcal{Q}(\theta_t^*, \omega_t) \leq & \langle \nabla_\theta \mathcal{Q}(\theta, \omega_t), \theta_t - \theta_t^* \rangle \\ \leq & \|\nabla_\theta \mathcal{Q}(\theta_t, \omega_t)\|_2 \cdot \|\theta_t - \theta_t^*\|_2, \end{aligned} \quad (13)$$

where $\theta_t^* = \arg\min_\theta \mathcal{Q}(\theta, \omega_t)$ and $\omega_t^* = \arg\min_\omega \mathcal{Q}(\theta_{t+1}, \omega)$. By combining Eqs. (12) and (13), we have

$$\mathcal{Q}(\theta_{t+1}, \omega_t) \leq \mathcal{Q}(\theta_t, \omega_t) - \frac{\eta}{\|\theta_t - \theta_t^*\|_2^2} \left(\mathcal{Q}(\theta_t, \omega_t) - \min_\theta \mathcal{Q}(\theta, \omega_t) \right)^2, \quad (14)$$

and similarly, we have

$$\mathcal{Q}(\theta_{t+1}, \omega_{t+1}) \leq \mathcal{Q}(\theta_{t+1}, \omega_t) - \frac{\eta}{\|\omega_t - \omega_t^*\|_2^2} \left(\mathcal{Q}(\theta_{t+1}, \omega_t) - \min_\omega \mathcal{Q}(\theta_{t+1}, \omega) \right)^2. \quad (15)$$

In particular, we have

$$\begin{aligned}\mathcal{Q}(\theta_{t+1},\omega_{t+1}) \leq & \mathcal{Q}(\theta_t,\omega_t) - \frac{\eta}{\|\theta_t-\theta_t^*\|_2^2}\left(\mathcal{Q}(\theta_t,\omega_t) - \min_\theta \mathcal{Q}(\theta,\omega_t)\right)^2 \\ & - \frac{\eta}{\|\omega_t-\omega_t^*\|_2^2}\left(\mathcal{Q}(\theta_{t+1},\omega_t) - \min_\omega \mathcal{Q}(\theta_{t+1},\omega)\right)^2.\end{aligned} \tag{16}$$

Therefore, the sequence $\mathcal{Q}(\theta_t,\omega_t)$ is monotonically decreasing. Since $\mathcal{Q}(\theta_t,\omega_t)$ is non-negative, it converges to some non-negative constant. By Eq. (16), we have

$$\begin{aligned}&\mathcal{Q}(\theta_{t+1},\omega_{t+1}) - \mathcal{Q}(\theta_t,\omega_t) \\ \geq & \frac{\eta}{\|\theta_t-\theta_t^*\|_2^2}\left(\mathcal{Q}(\theta_t,\omega_t) - \min_\theta \mathcal{Q}(\theta,\omega_t)\right)^2 + \frac{\eta}{\|\omega_t-\omega_t^*\|_2^2}\left(\mathcal{Q}(\theta_{t+1},\omega_t) - \min_\omega \mathcal{Q}(\theta_{t+1},\omega)\right)^2.\end{aligned} \tag{17}$$

Since the left-hand side tends to zero and the right-hand side is lower bounded by zero, by the sandwich theorem the sequences

$$\frac{\eta}{\|\theta_t-\theta_t^*\|_2^2}\left(\mathcal{Q}(\theta_t,\omega_t) - \min_\theta \mathcal{Q}(\theta,\omega_t)\right)^2$$

and

$$\frac{\eta}{\|\omega_t-\omega_t^*\|_2^2}\left(\mathcal{Q}(\theta_{t+1},\omega_t) - \min_\omega \mathcal{Q}(\theta_{t+1},\omega)\right)^2$$

tend to zero. We note that θ_t and ω_t are convergent sequences and are, therefore, also bounded. In addition, we recall that the sets $\{\arg\min_\theta \mathcal{Q}(\theta,\omega) \mid \omega \in \Omega\}$ and $\{\arg\min_\omega \mathcal{Q}(\theta,\omega) \mid \theta \in \Theta\}$ are well-defined and bounded. Hence, the terms $\|\theta_t-\theta_t^*\|_2^2$ and $\|\omega_t-\omega_t^*\|_2^2$ are bounded. Thus, we conclude that the sequences $(\mathcal{Q}(\theta_t,\omega_t) - \min_\theta \mathcal{Q}(\theta,\omega_t))^2$ and $(\mathcal{Q}(\theta_{t+1},\omega_t) - \min_\omega \mathcal{Q}(\theta_{t+1},\omega))^2$ tend to zero. In particular,

$$\begin{aligned}\lim_{t\to\infty} \mathcal{Q}(\theta_t,\omega_t) &= \lim_{t\to\infty} \min_\theta \mathcal{Q}(\theta,\omega_t) \\ \lim_{t\to\infty} \mathcal{Q}(\theta_{t+1},\omega_t) &= \lim_{t\to\infty} \min_\omega \mathcal{Q}(\theta_t,\omega)\end{aligned} \tag{18}$$

Since $\mathcal{Q}$ is a Lipschitz continuous function, we have (i) $\lim_{t\to\infty} \mathcal{Q}(\theta_{t+1},\omega_t) = \lim_{t\to\infty} \mathcal{Q}(\theta_t,\omega_t) = \mathcal{Q}(\hat{\theta},\hat{\omega})$, (ii) $\lim_{t\to\infty} \min_\theta \mathcal{Q}(\theta,\omega_t) = \min_\theta \mathcal{Q}(\theta,\hat{\omega})$ and (iii) $\lim_{t\to\infty} \min_\omega \mathcal{Q}(\theta_t,\omega) = \min_\omega \mathcal{Q}(\hat{\theta},\omega)$. Therefore, we finally conclude that $(\hat{\theta},\hat{\omega})$ is an equilibrium point of $\mathcal{Q}$. ■

Appendix B. Uniform Quantization

The uniform quantization method is fully described in Alg. 2. For a given function p, we denote by ∂p the estimated gradients of p w.r.t x. In Alg. 2, the estimated gradient of $\tilde{z}$ is computed as the gradient of $\min(\max(z_{init}, q_{\min}), q_{\max})$ (since $\partial \mathrm{round}(x) = 1$ when applying STE Bengio et al. (2013b)), which is simply $\mathbb{1}[z_{init} \in (q_{\min}, q_{\max})] \cdot \frac{\partial z_{init}}{\partial x}$, where $\frac{\partial z_{init}}{\partial x}$ is the gradient of z_{init} w.r.t x. $\partial \tilde{q}_i$ and ∂q are defined similarly, see lines 10-11 in Alg. 2.

Algorithm 2 The uniform quantization method (forward and backward passes)

Require: x is tensor to be quantized; r number of bits.

$q_{\min}, q_{\max} = 0, 2^r - 1$;
$x_{\min}, x_{\max} = \min_j\{x_j\}, \max_j\{x_j\}$;
$s = \frac{x_{\max} - x_{\min}}{q_{\max} - q_{\min}}$;
$z_{\text{init}} = \frac{q_{\min} - x_{\min}}{s}$;
$z = \min(\max(z_{\text{init}}, q_{\min}), q_{\max})$;
$\tilde{z} = \text{round}(z)$;
$\forall i: \ \tilde{q}_i = \tilde{z} + \frac{x_i}{s}$;
$\forall i: \ q_i = \text{round}(\min(\max(\tilde{q}_i, q_{\min}), q_{\max}))$;
$\partial \tilde{z} = \mathbb{1}[z_{init} \in (q_{\min}, q_{\max})] \cdot \frac{\partial z_{init}}{\partial x}$;
$\forall i: \ \partial \tilde{q}_i = \partial \tilde{z} + \frac{\partial (x_i/s)}{\partial x}$;
$\forall i: \ \partial q_i = \mathbb{1}[\tilde{q}_i \in (q_{\min}, q_{\max})] \cdot \partial \tilde{q}_i$;
return q, ∂q;

Appendix C. Qualitative Analysis

We provide a qualitative analysis of the advantage of our method over a simple neural network with a quantized representation layer. Each method learns a binarized feature map $b \circ F$. In this experiment, for each learned feature map F and a given ground-truth attribute $q_i(x)$, we compute $d_D(q_i; b \circ q \circ F)$ that measures whether it appears in the learned binarized representation layer $b \circ q \circ F$. In Figs. 4-6 we plot the values of $d_D(q_i; b \circ q \circ F)$ for each attribute in the dataset as a heatmap. We also report the number of attributes for which our method achieves a higher score (by at least $\epsilon = 0.05$) and vice versa.

2D Boxy	3D Boxy	Round	Vert Cyl	Horiz Cyl	Tail	Occluded	Beak
Head	Ear	Snout	Nose	Mouth	Hair	Face	Eye
Hand	Leg	Foot	Wing	Propeller	Jet engine	Window	Row Wind
Door	Headlight	Taillight	Side Mirror	Pedal	Handlebars	Sail	Mast
Leaf	Flower	Stem	Wool	Clear	Skin	Metal	Plastic
Shiny	Vegetation	Wood	Cloth	Hern	Rein	Exhaust	Trunk
Exhaust	Saddle	Shiny	Furn. Leg	Furn. Back	Furn. Seat	Furn. Arm	Glass
Screen	Arm	Torso	Wheel	Label	Leather	Jen Engine	Pot

2D Boxy	3D Boxy	Round	Vert Cyl	Horiz Cyl	Tail	Occluded	Beak
Head	Ear	Snout	Nose	Mouth	Hair	Face	Eye
Hand	Leg	Foot	Wing	Propeller	Jet engine	Window	Row Wind
Door	Headlight	Taillight	Side Mirror	Pedal	Handlebars	Sail	Mast
Leaf	Flower	Stem	Wool	Clear	Skin	Metal	Plastic
Shiny	Vegetation	Wood	Cloth	Hern	Rein	Exhaust	Trunk
Exhaust	Saddle	Shiny	Furn. Leg	Furn. Back	Furn. Seat	Furn. Arm	Glass
Screen	Arm	Torso	Wheel	Label	Leather	Jen Engine	Pot

Figure 4: **Heatmaps of $d_D(q_i; b \circ q \circ F)$ on the aYahoo dataset (Farhadi et al., 2009b).** In **(top)** we report the results of our method. **(bottom)** reports the results of a standard neural network with a quantized representation layer. Our method obtains a higher score on 23 attributes and a lower score on 4 attributes.

2D Boxy	3D Boxy	Round	Vert Cyl	Horiz Cyl	Tail	Occluded	Beak
Head	Ear	Snout	Nose	Mouth	Hair	Face	Eye
Hand	Leg	Foot	Wing	Propeller	Jet engine	Window	Row Wind
Door	Headlight	Taillight	Side Mirror	Pedal	Handlebars	Sail	Mast
Leaf	Flower	Stem	Wool	Clear	Skin	Metal	Plastic
Shiny	Vegetation	Wood	Cloth	Hern	Rein	Exhaust	Trunk
Exhaust	Saddle	Shiny	Furn. Leg	Furn. Back	Furn. Seat	Furn. Arm	Glass
Screen	Arm	Torso	Wheel	Label	Leather	Jen Engine	Pot

2D Boxy	3D Boxy	Round	Vert Cyl	Horiz Cyl	Tail	Occluded	Beak
Head	Ear	Snout	Nose	Mouth	Hair	Face	Eye
Hand	Leg	Foot	Wing	Propeller	Jet engine	Window	Row Wind
Door	Headlight	Taillight	Side Mirror	Pedal	Handlebars	Sail	Mast
Leaf	Flower	Stem	Wool	Clear	Skin	Metal	Plastic
Shiny	Vegetation	Wood	Cloth	Hern	Rein	Exhaust	Trunk
Exhaust	Saddle	Shiny	Furn. Leg	Furn. Back	Furn. Seat	Furn. Arm	Glass
Screen	Arm	Torso	Wheel	Label	Leather	Jen Engine	Pot

Figure 5: **Heatmaps of $d_D(q_i; b \circ q \circ F)$ on the aPascal dataset (Farhadi et al., 2009b).** In **(top)** we report the results of our method. **(bottom)** reports the results of a standard neural network with a quantized representation layer. Our method obtains a higher score on 38 attributes and a lower score on 3 attributes.

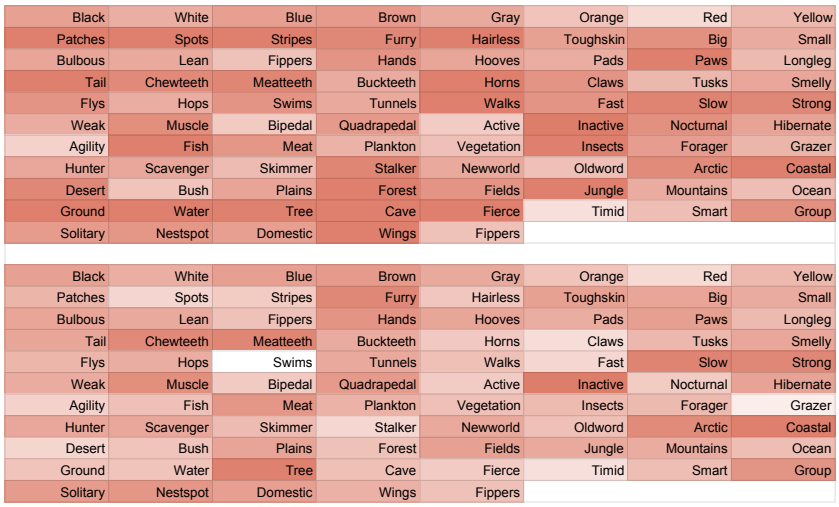

Figure 6: **Heatmaps of $d_D(q_i; b \circ q \circ F)$ on the AwA2 dataset (Xian et al., 2018).** In **(top)** we report the results of our method. **(bottom)** reports the results of a standard neural network with a quantized representation layer. Our method obtains a higher score on 48 attributes and a lower score on 3 attributes.

Appendix D. Training Dynamics

In the following, we show the training dynamics over aPascal and aYahoo datasets. As can be seen, as a general tendency, the fidelity score increases in correlation with the intersection regularization loss (IR Loss) decreases. While during most of the training process both metrics improve together, at later stages they seem to fluctuate in a narrow band in a matter that is not always correlated. The cross-entropy (CE) loss and the accuracy constantly improve from epoch to epoch. Therefore, we do not see a clear tradeoff between the IR loss and the CE loss, at least in the first 12 epochs. =

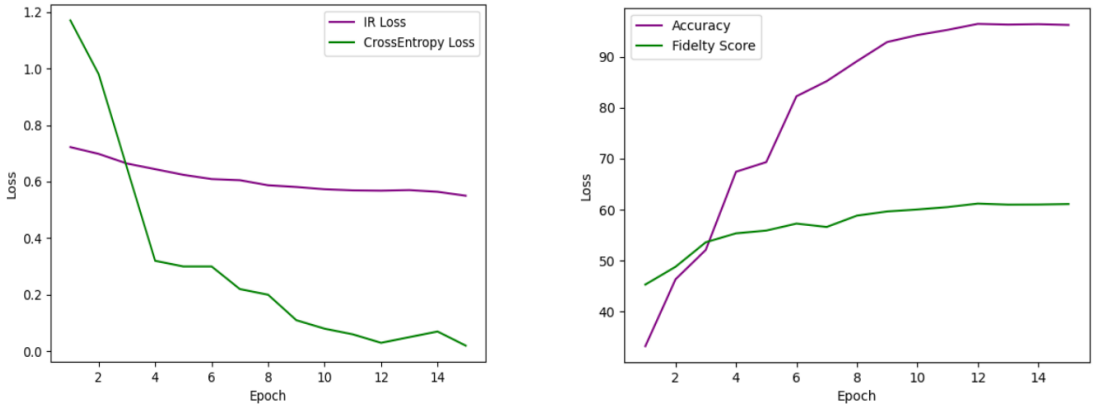

Figure 7: **The training dynamics over aYahoo dataset.**

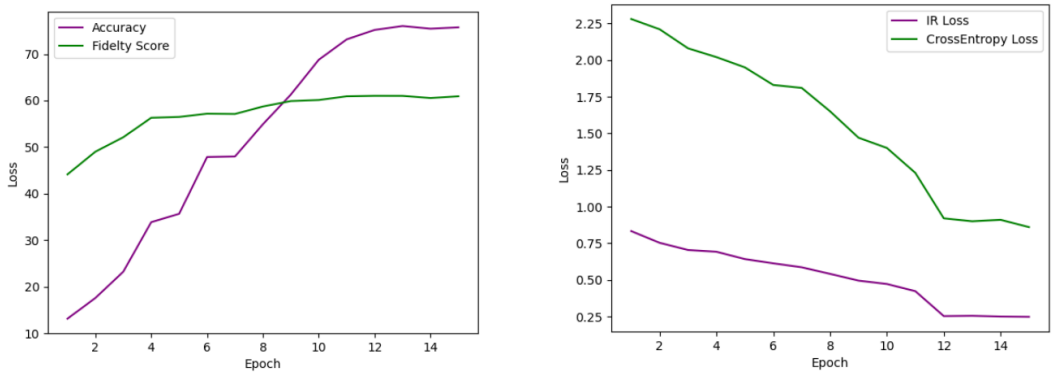

Figure 8: **The training dynamics over aPascal dataset.**